Switching and redox isomerism in first-row transition metal complexes containing redox active Schiff base ligands

Supplementary information

Ashok Sasmal[a], Eugenio Garribba[b], Carlos J. Gómez-García[c], Cédric Desplanches[d],

Samiran Mitra*[a]

[a]Department of Chemistry, Jadavpur University, Raja S.C. Mullick Road, Kolkata-700032, West Bengal, India

[b]Department of Chemistry and Pharmacy, and Center for Biotechnology Development and Biodiversity Research, University of Sassari, Via Vienna 2, I-07100 Sassari, Italy

[c]Institutode Ciencia Molecular (ICMol), Universidad de Valencia, ParqueCientífico, 46980 Paterna, Spain

[d]CNRS, Université de Bordeaux, ICMCB, 87 Avenue du Dr. A. Schweitzer, Pessac, F-33608, France

** Corresponding author: Tel: + 91-33-2414 6666 (Extn. 2779); fax: + 91-33-2414 6414*

E-mail address: samiranju92@gmail.com

UV-Vis spectroscopy of the complexes

In order to obtain more information on the electronic distribution, the UV-Vis spectra of all the neutral complexes were recorded in acetonitrile (Fig. S1). The more important bands appearing in the electronic spectra of all the members of the ML_2 series are listed in Table 3. Spectra recorded in acetonitrile solution at room temperature where different tautomeric forms of the complexes exist, show features which are characteristic of the charge distributions. Complexes **1** and **3** exhibit absorption patterns with several bands and shoulders. The high energy bands around ca. 294-344 nm are due to (O, N → Mn^{III} and Co^{III}) LMCT transitions. The broad bands around 500-650 nm are due to spin allowed ($\Delta S = 0$) d-d transitions. The extra band is attributed to spin-orbit coupling effect. There is a band due to low energy intra ligand transitions around ca. 802 nm and 915 nm characteristic of the $[Mn^{III}(L^{2-})(L^{-})]$ / $[Co^{III}(L^{2-})(L^{-})]$and $[Mn^{IV}(L^{-})_2]$ / $[Co^{II}(L^{-})_2]$ species respectively. The complex **2** shows a sharp LMCT band at *ca.* 391 nm. The band at ca. 512 nm is due to spin allowed *d-d* transition. There is broad band in the range ca. 600 to 900 nm due to low energy intra ligand transition of $[Fe^{II}(L^{-})_2]$ species.[1] The zinc and nickel complexes show similar absorption patterns. The band around ca.350-500 nm is due to spin-orbit coupling. The bands at ca. 700-900 nm are due to low energy intra ligand transition in ligand-based redox isomers $[Zn^{II}(L^{2-})(L^{0})]$ / $[Zn^{II}(L^{-})_2]$. The complex shows a broad band at 600 nm due to *d-d* transitions $^2E_g \rightarrow {}^2T_{2g}$. There is also a band at 366 nm due to MLCT transitions. The bands at ca. 700-900 nm are due to low energy intra ligand transition in ligand-based redox isomer $[Cu^{II}(L^{2-})(L^{0})]/[Cu^{II}(L^{-})_2)]$.

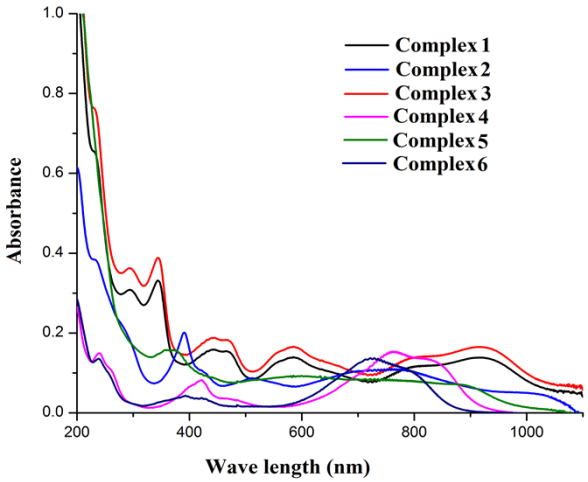

Fig. S1. UV-vis spectra of the complexes recorded in acetonitrile solutions.

Table S1. Absorption data of complexes **1**-**6**.

Complex	λ_{max}/nm (ε/M^{-1} cm^{-1})
1	232 (8730), 294 (4130), 344(4435), 443 (2110), 468(2050), 584(1810), 802(1550), 915(1850)
2	232(5100), 391(2660), 512(1140), 774(1430)
3	231(10220), 295(4845), 344(5200), 441(2510), 468(2450), 584 (2190), 800(1850), 920(2214)
4	239(1980), 420(1080), 764(2030), 823(1790)
5	366 (2070), 585 (1260)
6	238(1780), 393(540), 426(487), 723(1780)

1. L. Hu, W. Liu, C. -H. Li, X. -H. Zhou, J. -L. Zuo, *Eur. J. Inorg. Chem.* 2013, 6037–6048.

Table S2. Selected bond distances (Å) and bond angles (°) of complex 1

Mn1-O1	1.908(2)	C7-C12	1.409(4)
Mn1-O2	1.919(2)	C7-C8	1.431(4)
Mn1-O3	1.8968(19)	C8-C9	1.425(4)
Mn1-O4	1.885(2)	C9-C10	1.379(4)
Mn1-N1	1.903(2)	C10-C11	1.419(4)
Mn1-N2	1.917(2)	C11-C12	1.366(4)
O1-C2	1.316(3)	C13-C14	1.422(4)
O2-C8	1.309(3)	C13-C18	1.404(4)
O3-C20	1.311(3)	C14-C15	1.392(4)
O4-C14	1.316(3)	C15-C16	1.362(4)
N1-C1	1.380(3)	C16-C17	1.393(4)
N1-C7	1.361(3)	C17-C18	1.371(4)
N2-C13	1.383(3)	C19-C24	1.408(4)
N2-C19	1.373(3)	C19-C20	1.423(3)
Cl1-C5	1.741(3)	C20-C21	1.421(4)
Cl2-C17	1.729(3)	C21-C22	1.374(4)
C1-C6	1.406(4)	C22-C23	1.421(4)
C1-C2	1.409(4)	C23-C24	1.367(4)
C2-C3	1.397(4)	C21-C25	1.527(4)
C3-C4	1.381(5)	C9-C28	1.524(4)
C4-C5	1.392(4)	C11-C27	1.524(4)
C5-C6	1.366(4)	C23-C26	1.531(4)
O1-Mn1-O2	164.59(9)	O4-Mn1-N2	83.57(9)
O1-Mn1-O3	92.89(8)	N1-Mn1-N2	177.83(9)
O1-Mn1-O4	92.12(9)	N1-C7-C12	129.0(2)
O1-Mn1-N1	82.99(9)	N1-C1-C6	128.2(2)
O1-Mn1-N2	94.90(9)	N2-C13-C18	130.0(2)
O2-Mn1-O3	88.16(8)	N2-C19-C24	129.4(2)
O2-Mn1-O4	90.74(9)	O1-C2-C1	117.9(2)
O2-Mn1-N1	81.66(9)	O2-C8-C7	116.4(2)
O2-Mn1-N2	100.47(9)	O3-C20-C19	117.1(2)
O3-Mn1-O4	165.08(8)	O4-C14-C13	118.5(2)
O3-Mn1-N1	98.55(9)	C1-N1-C7	130.1(2)
O3-Mn1-N2	82.01(9)	C13-N2-C19	130.5(2)
O4-Mn1-N1	96.01(9)		

Table S3. Selected bond distances (Å) and bond angles (°) of complex 2

Fe1-O1	1.900(3)	C7-C8	1.417(6)
Fe1-O2	1.900(3)	C7-C12	1.409(7)
Fe1-O3	1.897(3)	C8-C9	1.426(7)
Fe1-O4	1.891(3)	C9-C10	1.372(7)
Fe1-N1	1.897(4)	C10-C11	1.422(6)
Fe1-N2	1.907(4)	C11-C12	1.363(7)
O1-C2	1.316(6)	C13-C14	1.414(6)
O2-C8	1.314(5)	C13-C18	1.396(6)
O3-C14	1.313(6)	C14-C15	1.384(7)
O4-C20	1.311(6)	C15-C16	1.355(8)
N1-C1	1.382(6)	C16-C17	1.392(9)
N1-C7	1.376(6)	C17-C18	1.379(6)
N2-C13	1.386(6)	C19-C20	1.422(6)
N2-C19	1.358(6)	C19-C24	1.409(7)
Cl1-C5	1.747(5)	C20-C21	1.421(6)
Cl2-C17	1.737(5)	C21-C22	1.368(7)
C1-C2	1.411(7)	C22-C23	1.423(6)
C1-C6	1.392(6)	C23-C24	1.365(6)
C2-C3	1.393(8)	C9-C37	1.520(7)
C3-C4	1.353(8)	C11-C33	1.524(7)
C4-C5	1.405(8)	C21-C25	1.529(6)
C5-C6	1.369(6)	C23-C29	1.523(7)
O1-Fe1-O2	164.97(14)	O4-Fe1-N2	82.21(15)
O1-Fe1-O3	91.87(15)	N1-Fe1-N2	176.76(15)
O1-Fe1-O4	91.13(15)	C1-N1-C7	129.7(4)
O1-Fe1-N1	82.80(15)	C13-N2-C19	130.7(4)
O1-Fe1-N2	98.04(15)	N1-C1-C6	109.8(4)
O2-Fe1-O3	91.31(14)	N1-C7-C12	128.9(4)
O2-Fe1-O4	89.47(14)	N2-C13-C18	128.8(4)
O2-Fe1-N1	82.18(14)	N2-C19-C24	130.0(4)
O2-Fe1-N2	96.91(14)	O1-C2-C1	118.4(5)
O3-Fe1-O4	165.42(15)	O2-C8-C7	116.6(4)
O3-Fe1-N1	99.88(15)	O3-C14-C13	118.2(4)
O3-Fe1-N2	83.24(15)	O4-C20-C19	117.4(4)
O4-Fe1-N1	94.66(15)		

Table S4. Selected bond distances (Å) and bond angles (°) of complex 3RT

Co1-O1	1.888(2)	C7-C8	1.425(5)
Co1-O2	1.879(2)	C7-C12	1.414(5)
Co1-O3	1.907(2)	C8-C9	1.427(4)
Co1-O4	1.914(2)	C9-C10	1.373(5)
Co1-N1	1.861(2)	C10-C11	1.420(5)
Co1-N2	1.867(2)	C11-C12	1.362(5)
Cl1-C5	1.734(4)	C13-C14	1.445(5)
Cl2-C17	1.735(4)	C13-C18	1.405(5)
O1-C2	1.322(4)	C14-C15	1.416(5)
O2-C8	1.322(4)	C15-C16	1.352(6)
O3-C14	1.292(4)	C16-C17	1.412(6)
O4-C20	1.278(4)	C17-C18	1.358(5)
N1-C1	1.365(4)	C19-C20	1.462(4)
N1-C7	1.357(4)	C19-C24	1.419(4)
N2-C13	1.361(4)	C20-C21	1.430(5)
N2-C19	1.338(4)	C21-C22	1.368(5)
C1-C2	1.428(5)	C22-C23	1.447(5)
C1-C6	1.405(5)	C23-C24	1.349(5)
C2-C3	1.391(5)	C9-C33	1.525(5)
C3-C4	1.367(5)	C11-C37	1.530(5)
C4-C5	1.400(6)	C21-C25	1.532(5)
C5-C6	1.366(5)	C23-C29	1.526(5)
O1-Co1-O2	171.68(10)	O4-Co1-N2	84.30(10)
O1-Co1-O3	91.67(10)	N1-Co1-N2	177.34(11)
O1-Co1-O4	90.49(10)	N1-C1-C6	128.6(3)
O1-Co1-N1	86.18(10)	N1-C7-C12	129.0(3)
O1-Co1-N2	96.25(10)	N2-C13-C18	128.6(3)
O2-Co1-O3	90.24(10)	N2-C19-C24	129.1(3)
O2-Co1-O4	89.03(10)	O1-C2-C1	118.6(3)
O2-Co1-N1	85.58(11)	O2-C8-C7	118.2(3)
O2-Co1-N2	91.97(11)	O3-C14-C13	119.9(3)
O3-Co1-O4	169.94(10)	O4-C20-C19	117.7(3)
O3-Co1-N1	95.34(10)	C1-N1-C7	133.7(3)
O3-Co1-N2	85.70(10)	C13-N2-C19	132.1(3)
O4-Co1-N1	94.61(10)		

Table S5. Selected bond distances (Å) and bond angles (°) of complex 3LT

Co1-O1	1.904(2)	C7-C8	1.463(4)
Co1-O2	1.908(2)	C7-C12	1.422(4)
Co1-O3	1.890(2)	C8-C9	1.440(4)
Co1-O4	1.882(2)	C9-C10	1.365(5)
Co1-N1	1.862(2)	C10-C11	1.445(4)
Co1-N2	1.862(2)	C11-C12	1.358(4)
Cl1-C5	1.740(4)	C13-C14	1.435(4)
Cl2-C17	1.743(3)	C13-C18	1.406(4)
O1-C1	1.297(4)	C14-C15	1.403(5)
O2-C8	1.282(3)	C15-C16	1.375(5)
O3-C14	1.318(4)	C16-C17	1.409(5)
O4-C20	1.314(3)	C17-C18	1.366(5)
N1-C1	1.359(4)	C19-C20	1.432(4)
N1-C7	1.344(4)	C19-C24	1.417(4)
N2-C13	1.371(4)	C20-C21	1.417(4)
N2-C19	1.361(4)	C21-C22	1.382(5)
C1-C2	1.443(5)	C22-C23	1.419(5)
C1-C6	1.413(5)	C23-C24	1.372(4)
C2-C3	1.420(5)	C9-C25	1.534(4)
C3-C4	1.362(5)	C11-C29	1.533(4)
C4-C5	1.417(5)	C21-C33	1.542(5)
C5-C6	1.364(5)	C23-C37	1.534(5)
O1-Co1-O2	170.34(9)	O4-Co1-N2	85.79(10)
O1-Co1-O3	91.58(10)	N1-Co1-N2	177.56(11)
O1-Co1-O4	90.45(10)	C1-N1-C7	131.9(3)
O1-Co1-N1	85.73(10)	C13-N2-C19	133.8(2)
O1-Co1-N2	95.20(10)	N1-C1-C6	128.5(3)
O2-Co1-O3	90.61(9)	N1-C7-C12	129.2(3)
O2-Co1-O4	88.69(9)	N2-C13-C18	128.5(3)
O2-Co1-N1	84.69(10)	N2-C19-C24	128.2(3)
O2-Co1-N2	94.33(10)	O1-C2-C1	119.6(3)
O3-Co1-O4	171.90(9)	O2-C8-C7	117.8(2)
O3-Co1-N1	96.02(10)	O3-C14-C13	118.8(3)
O3-Co1-N2	86.22(10)	O4-C20-C19	118.3(3)
O4-Co1-N1	91.95(10)		

Table S6. Selected bond distances (Å) and bond angles (°) of complex 4

Ni1-O1	2.038(2)	C7-C12	1.427(4)
Ni1-O2	2.089(2)	C7-C8	1.483(4)
Ni1-O3	2.022(2)	C8-C9	1.448(4)
Ni1-O4	2.036(2)	C9-C10	1.352(4)
Ni1-N1	2.016(2)	C10-C11	1.436(4)
Ni1-N2	2.029(2)	C11-C12	1.344(4)
O1-C1	1.269(3)	C13-C14	1.459(4)
O2-C8	1.256(3)	C13-C18	1.421(4)
O3-C14	1.269(3)	C14-C15	1.422(4)
O4-C20	1.255(3)	C15-C16	1.343(4)
N1-C1	1.353(3)	C16-C17	1.417(4)
N1-C7	1.329(3)	C17-C18	1.344(4)
N2-C13	1.360(3)	C19-C24	1.431(4)
N2-C19	1.340(4)	C19-C20	1.480(4)
Cl1-C5	1.742(3)	C20-C21	1.447(4)
Cl2-C17	1.732(3)	C21-C22	1.352(4)
C1-C6	1.415(4)	C22-C23	1.431(4)
C1-C2	1.461(4)	C23-C24	1.350(4)
C2-C3	1.427(4)	C9-C28	1.539(4)
C3-C4	1.349(5)	C11-C27	1.532(4)
C4-C5	1.411(4)	C21-C26	1.531(4)
C5-C6	1.358(4)	C23-C25	1.529(4)
O1-Ni1-O2	160.20(8)	O4-Ni1-N2	79.89(8)
O1-Ni1-O3	91.43(8)	N1-Ni1-N2	177.16(9)
O1-Ni1-O4	94.57(8)	N1-C1-C6	128.0(2)
O1-Ni1-N1	81.19(8)	N1-C7-C12	128.7(2)
O1-Ni1-N2	100.95(8)	N2-C13-C18	129.1(2)
O2-Ni1-O3	92.73(8)	N2-C19-C24	129.0(2)
O2-Ni1-O4	87.45(8)	O1-C2-C1	120.8(2)
O2-Ni1-N1	79.03(8)	O2-C8-C7	119.3(2)
O2-Ni1-N2	98.80(8)	O3-C14-C13	122.0(2)
O3-Ni1-O4	161.74(8)	O4-C20-C19	119.6(2)
O3-Ni1-N1	99.85(9)	C1-N1-C7	130.9(2)
O3-Ni1-N2	82.04(8)	C13-N2-C19	132.7(2)
O4-Ni1-N1	98.11(8)		

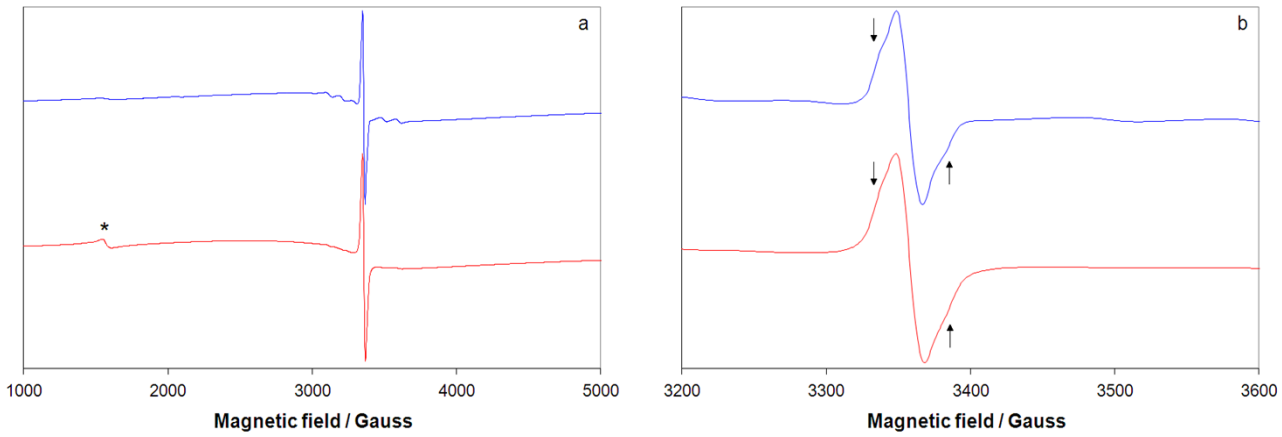

Fig. S2. (a) X-band EPR spectra of a polycrystalline sample of **2** at 298 K (blue) and 77 K (red). An asterisk indicates the forbidden $\Delta M_S = \pm 2$ transition. (b) Close view of the $g \approx 2$ region at 298 K (blue) and 77 K (red). The arrows indicate the position of the absorption due to the triplet state (S = 1).

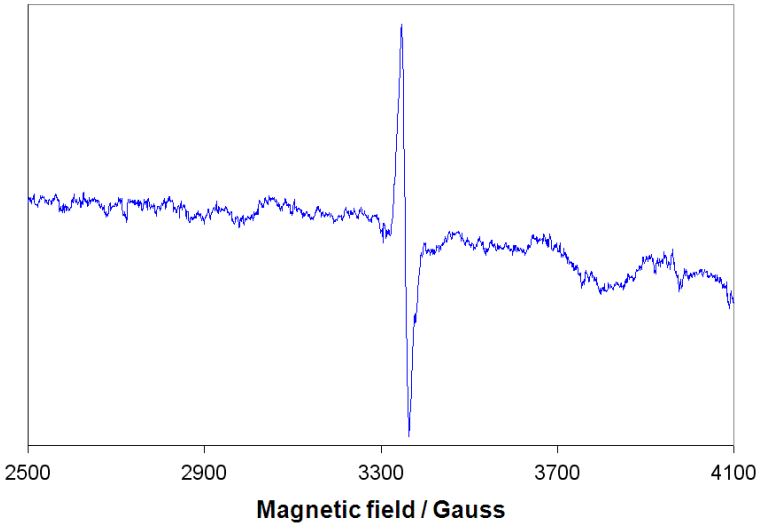

Fig. S3. X-band EPR spectrum of **2** dissolved in a mixture CH_2Cl_2/toluene (60:40 v/v).

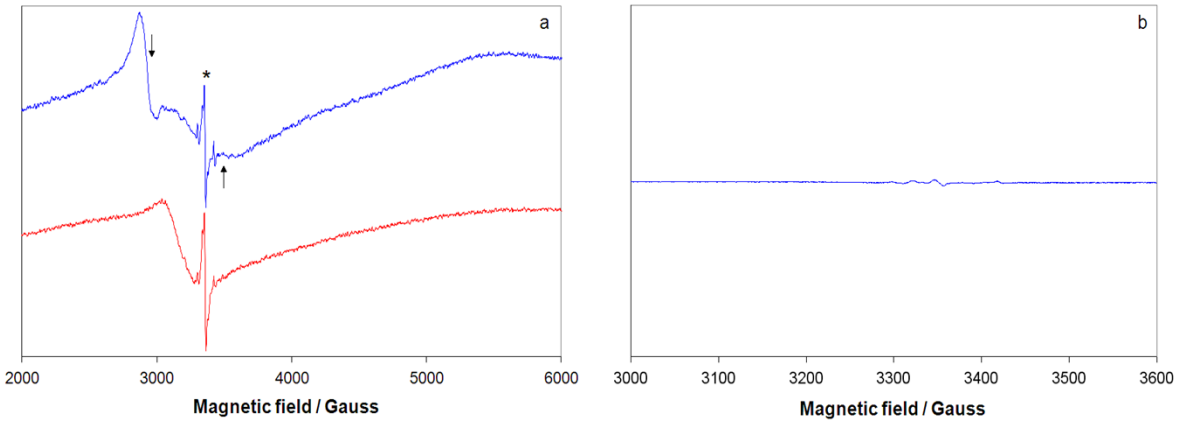

Fig. S4. (a) X-band EPR spectra of the polycrystalline complex **1** at 298 K (blue) and 77 K (red). The asterisk and the arrows indicate the lines due to the small fraction of $[Ni^{III}(L^{2-})(L^{-})]$ complex (b) X-band EPR spectrum of **4** dissolved in a mixture of CH_2Cl_2/toluene (60:40 v/v).

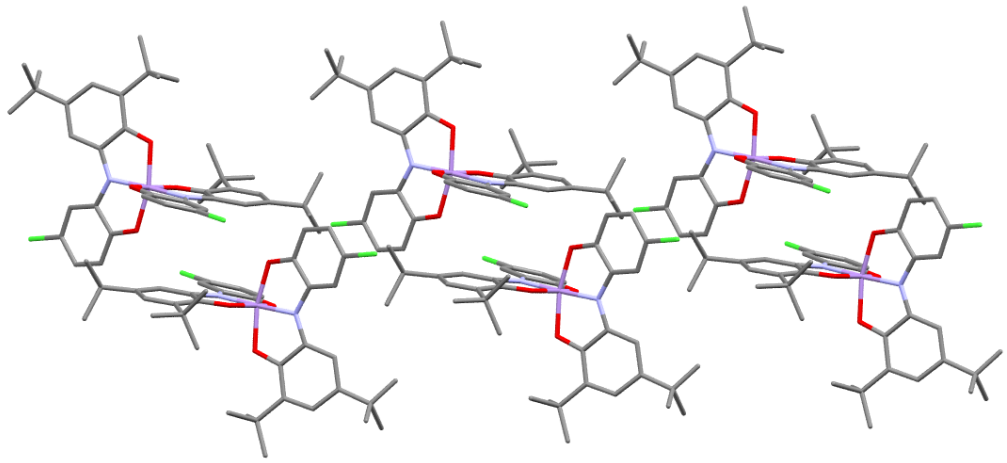

Fig. S5. Packing of MnL_2 complex extented along bc plan with π-π interaction between less twist ligand.

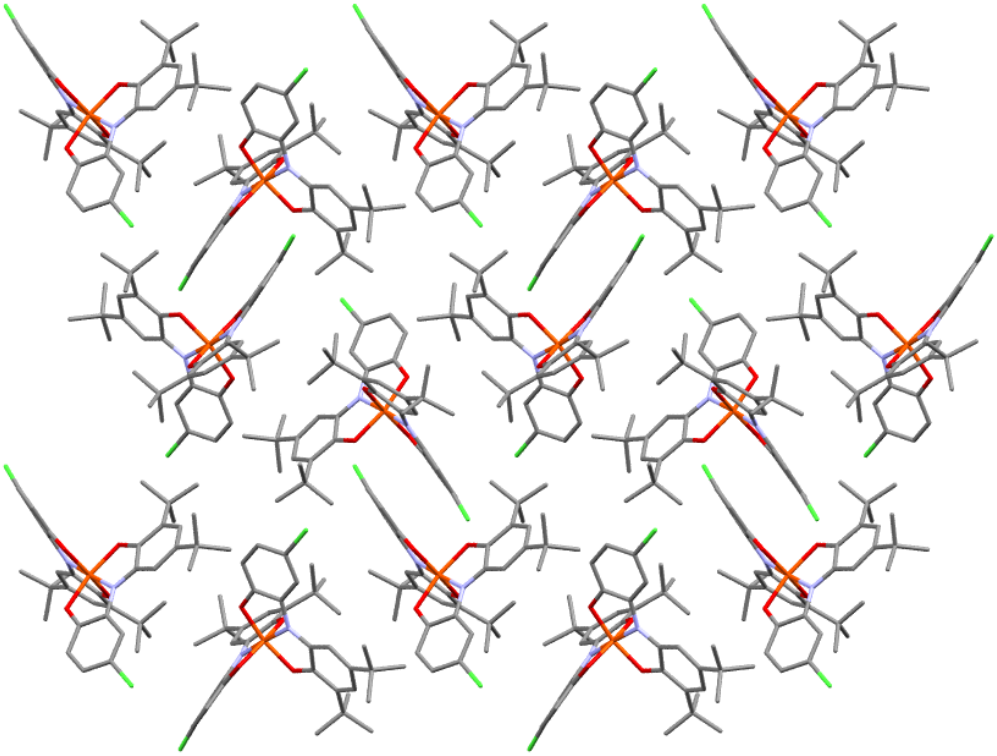

Fig. S6. Packing diagram of FeL_2 complex

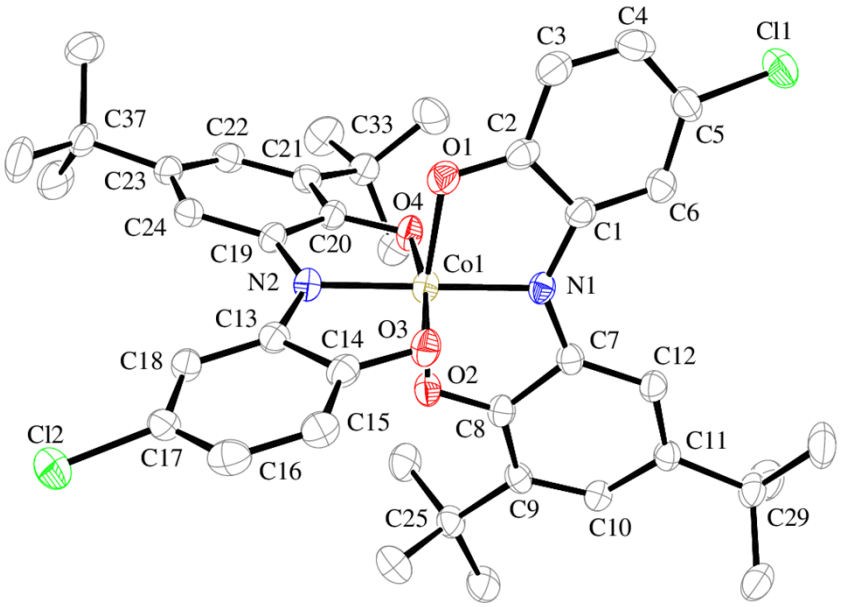

Fig. S7. Diagram of CoL_2 complex at 150K

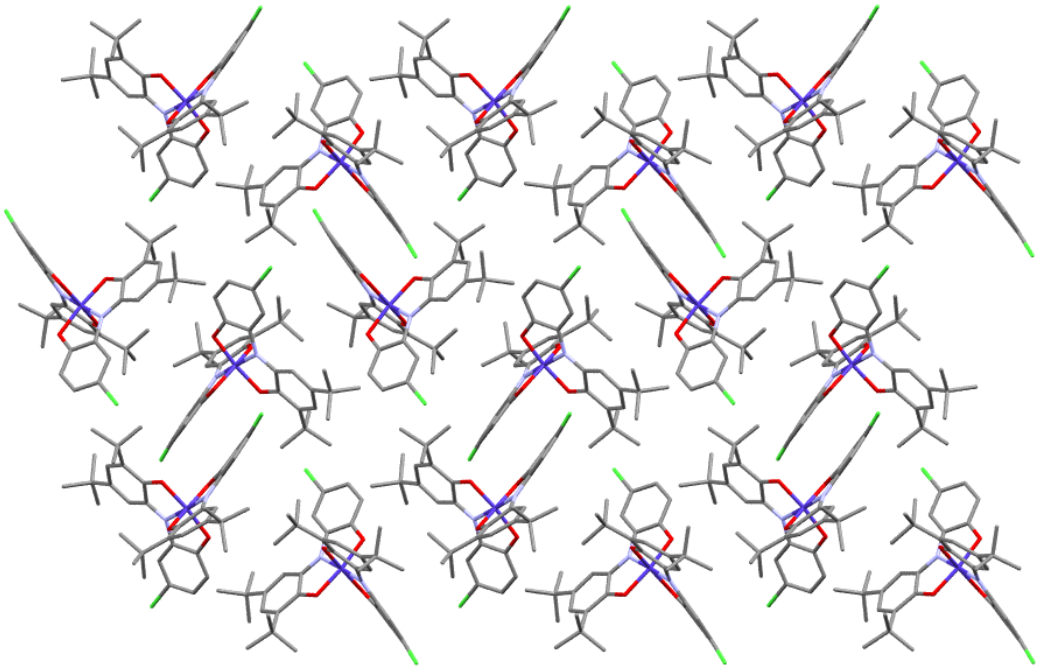

Fig. S8. Packing diagram of FeL_2 complex

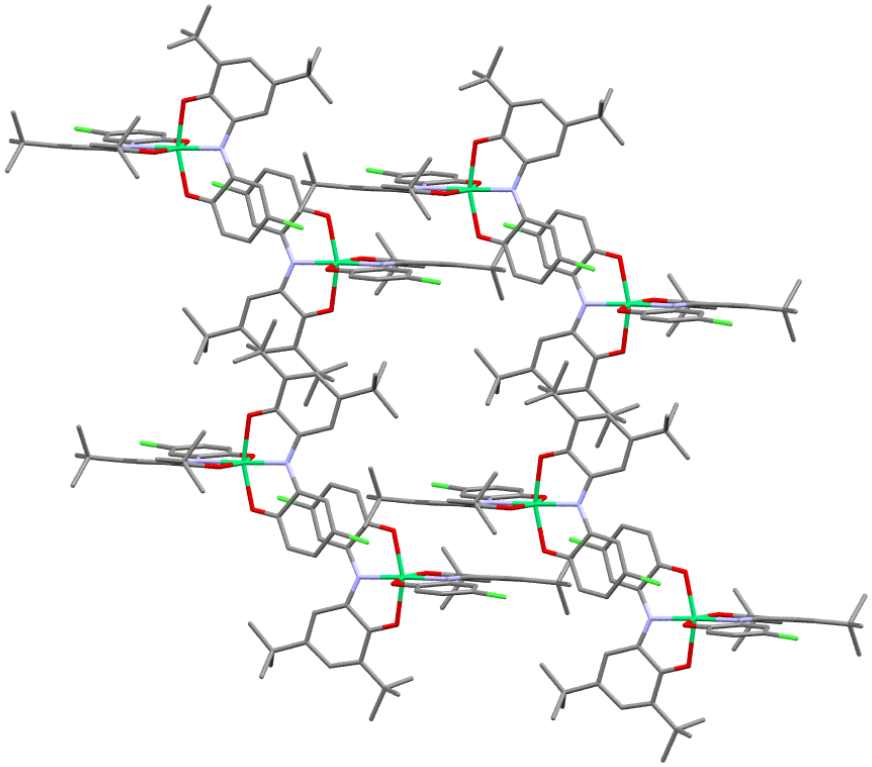

Fig. S9. Packing of NiL_2 complex extented along bc plan with π-π interaction between less twist ligand.

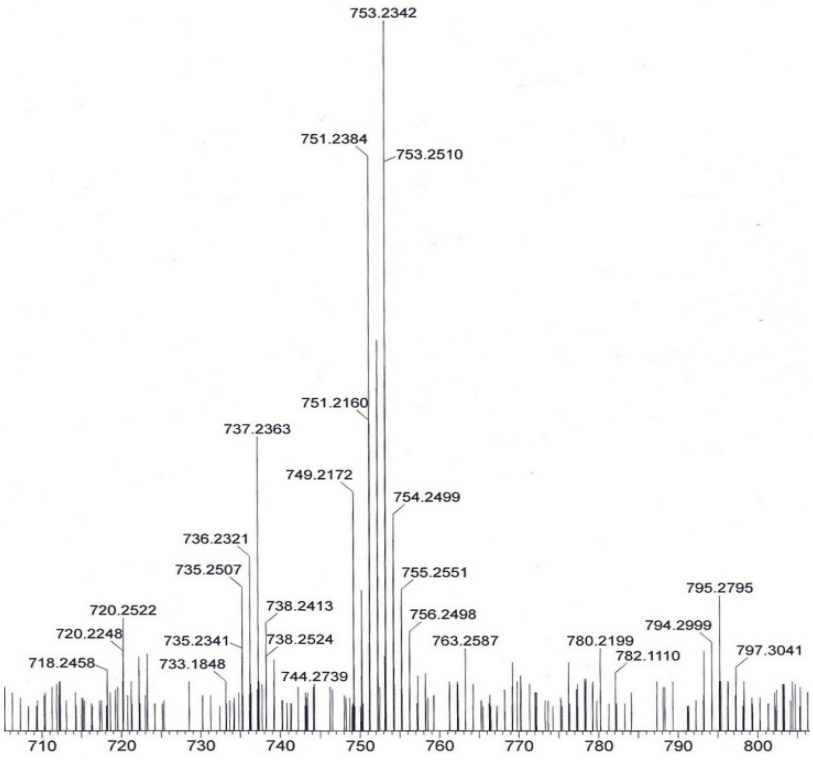

Fig. S10. Mass spectrum of CuL_2 complex

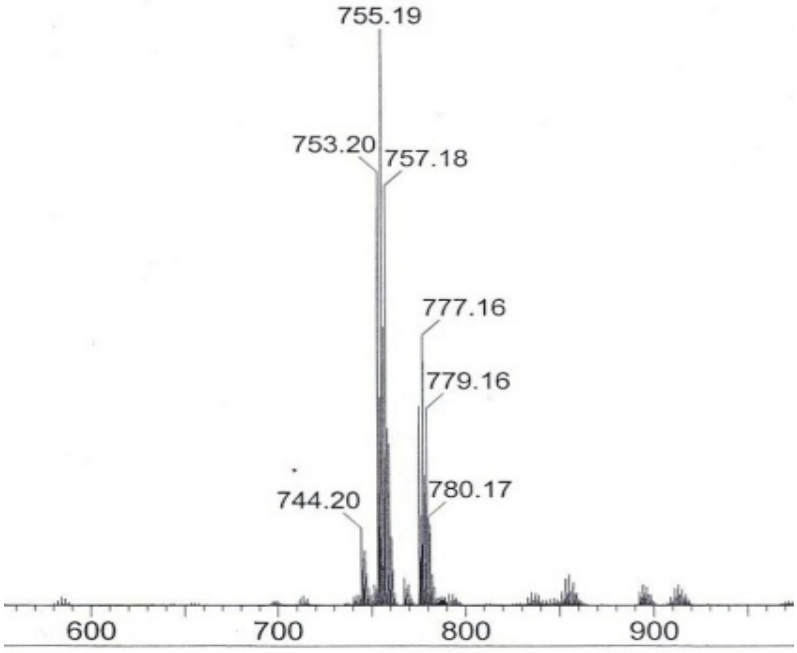

Fig. S11. Mass spectrum of ZnL_2 complex

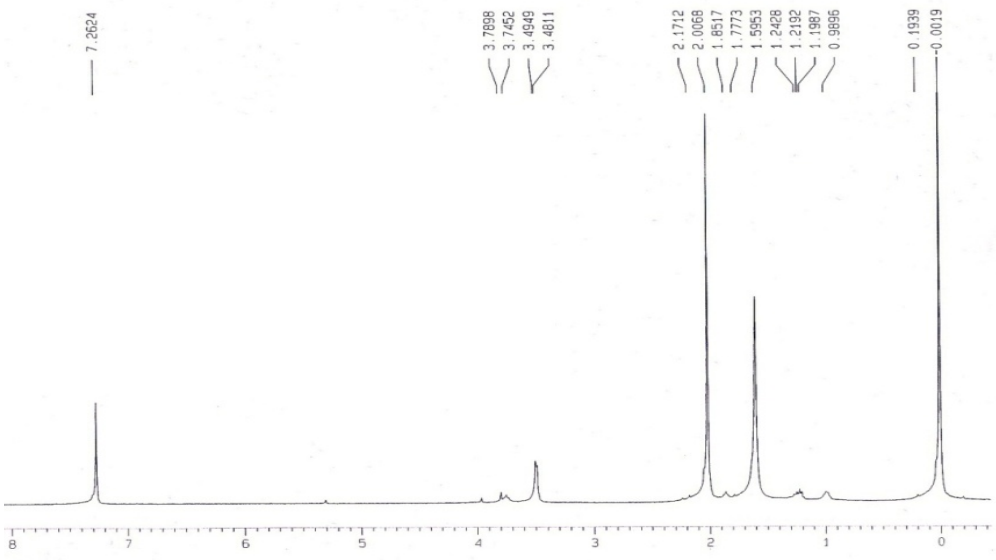

Fig. S12. NMR spectrum of complex **1** in $CDCl_3$

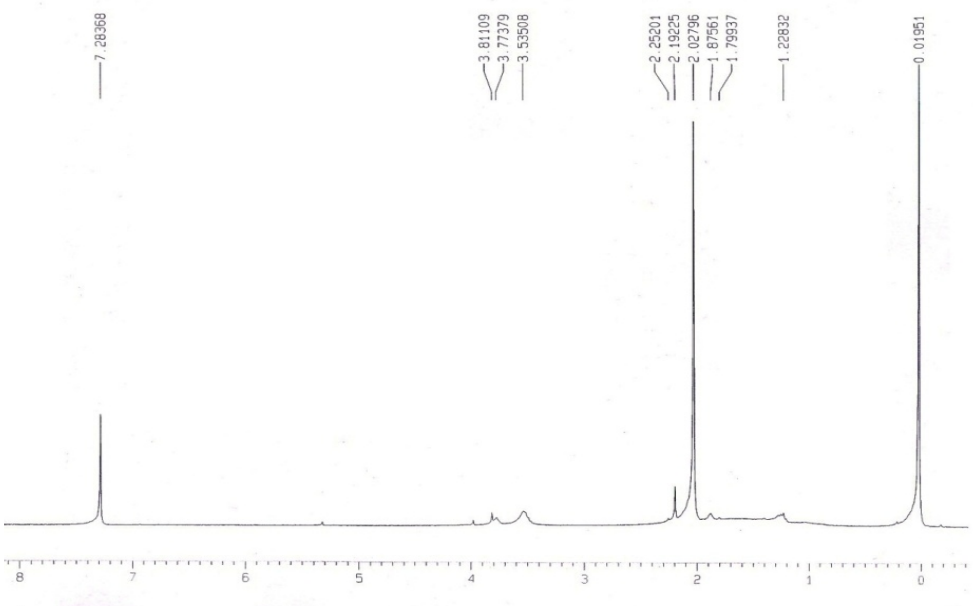

Fig. S13. NMR spectrum of complex **2** in $CDCl_3$

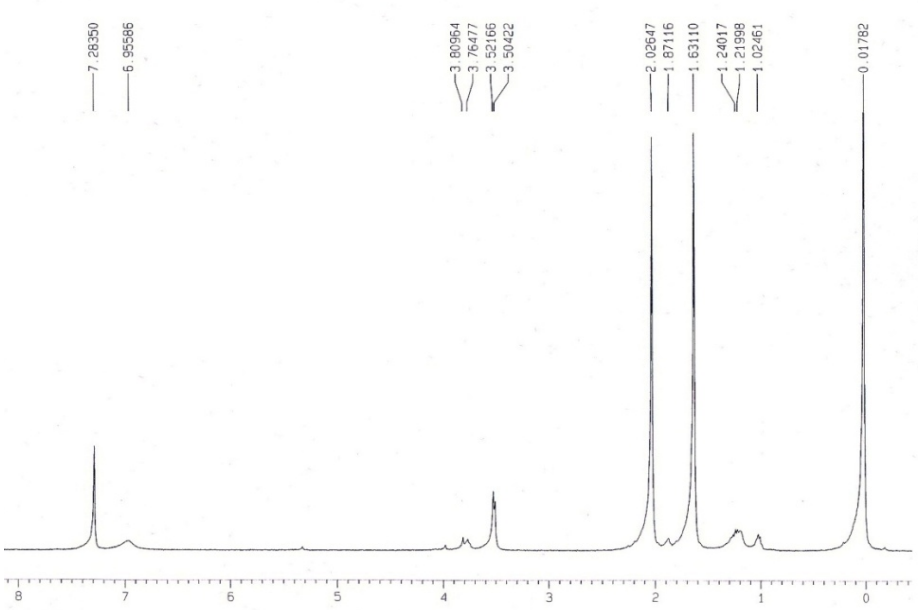

Fig. S14. NMR spectrum of complex **3** in $CDCl_3$

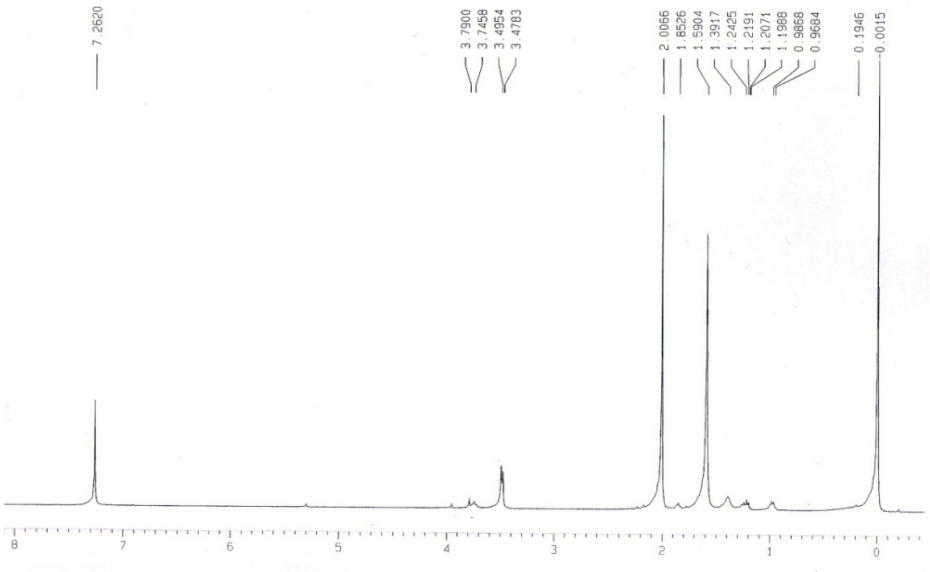

Fig. S15. NMR spectrum of complex **4** in $CDCl_3$

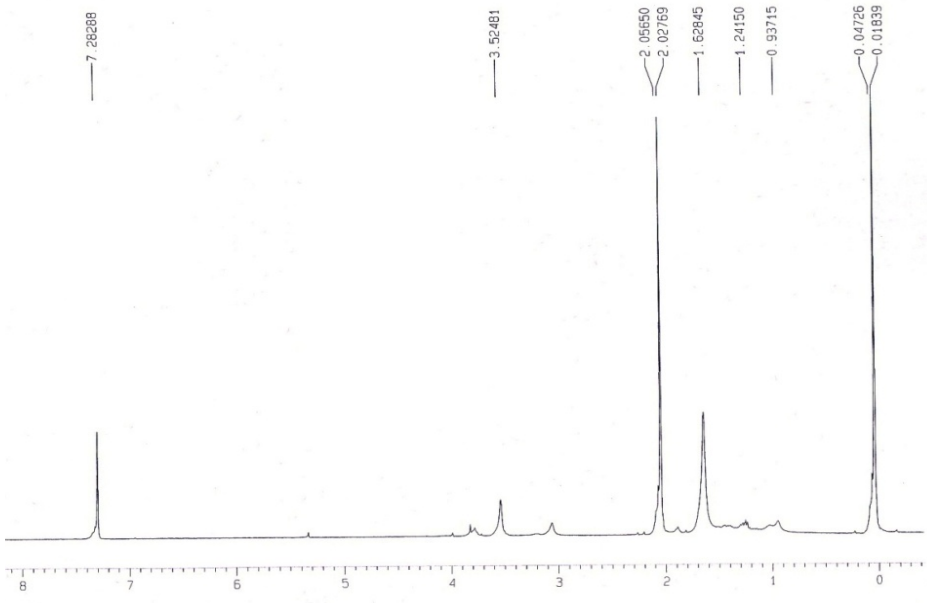

Fig. S16. NMR spectrum of complex **5** in $CDCl_3$

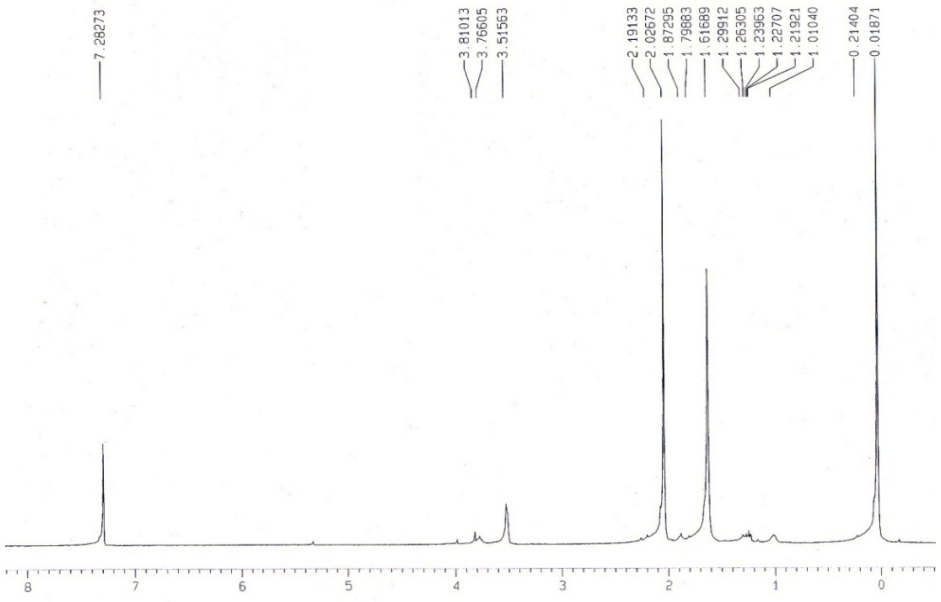

Fig. S17. NMR spectrum of complex **6** in $CDCl_3$

X-ray powder diffraction (XRPD) measurements

Phase purity of samples 1 - 4 were established by XRPD. Samples of 1 - 6 were lightly ground in an agate mortar and pestle and filled into 0.7 mm borosilicate capillaries. Data were collected at room temperature in the 2θ range 5-50° on a Bruker D8 advance powder diffractometer using Cu Kα radiation (λ = 1.54056 Å). The comparison of the measured powder diffraction patterns (red) and calculated from single-crystal data (black) of 1-4 have been shown. The measured powder diffraction patterns of 5 and 6 have also been shown.

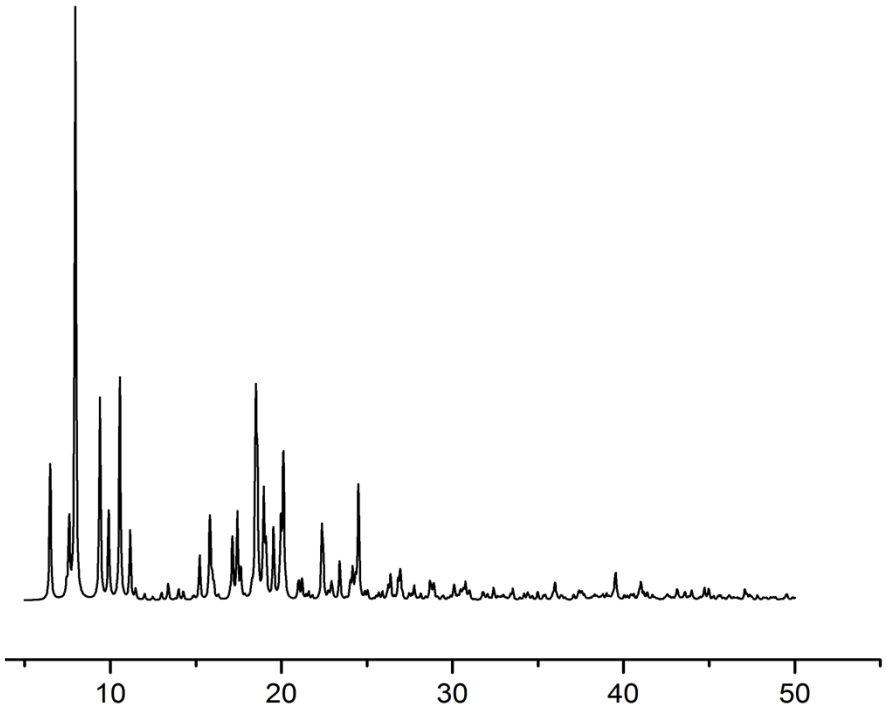

Figure S18: Simulated X-ray diffraction pattern of complex **1**

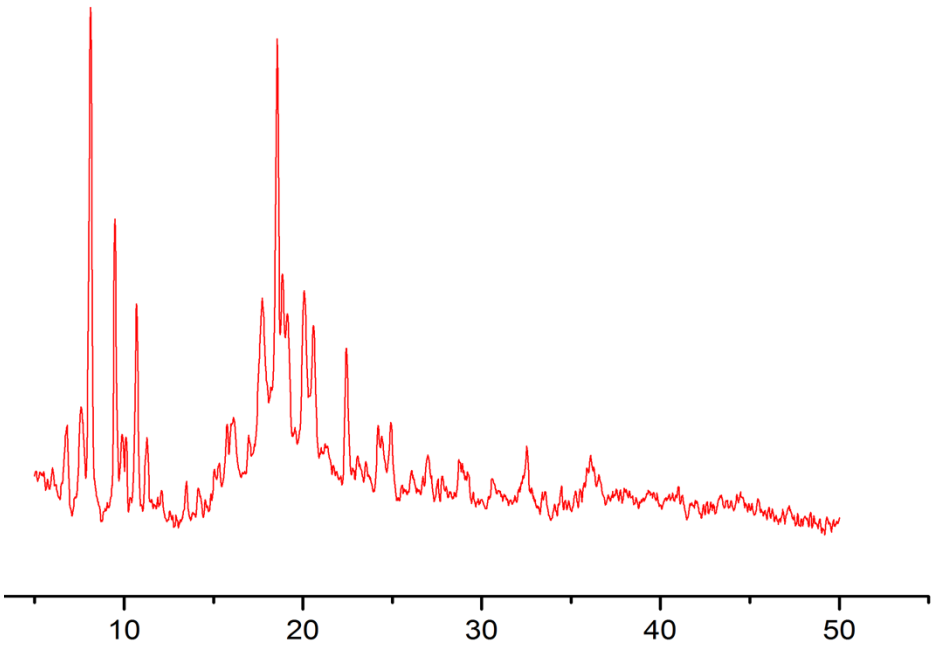

Figure S19: Powder X-ray diffraction pattern of complex **1**

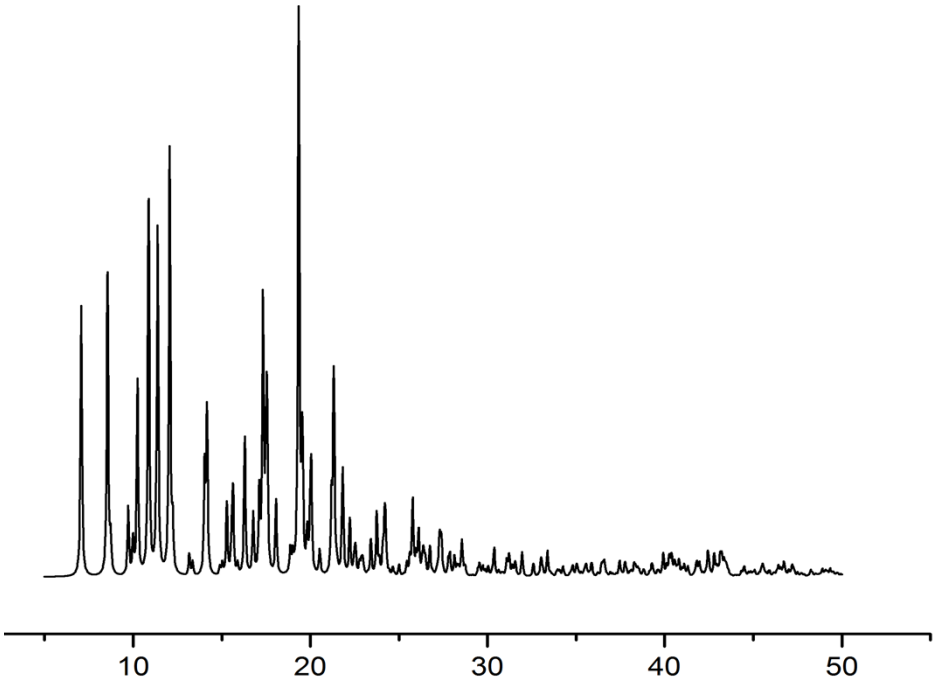

Figure S20: Simulated X-ray diffraction pattern of complex **2**

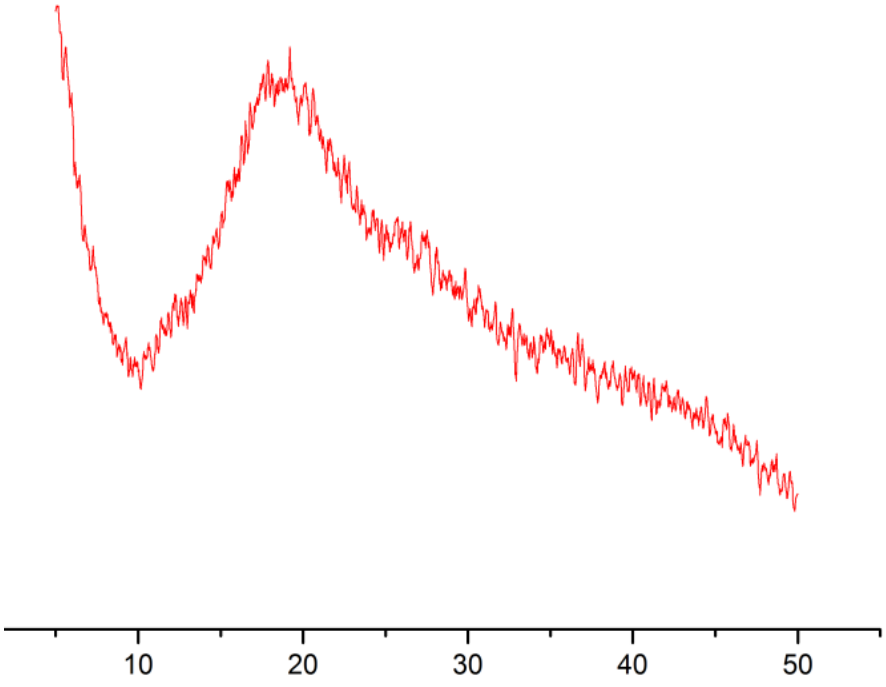

Figure S21: Powder X-ray diffraction pattern of complex **2**

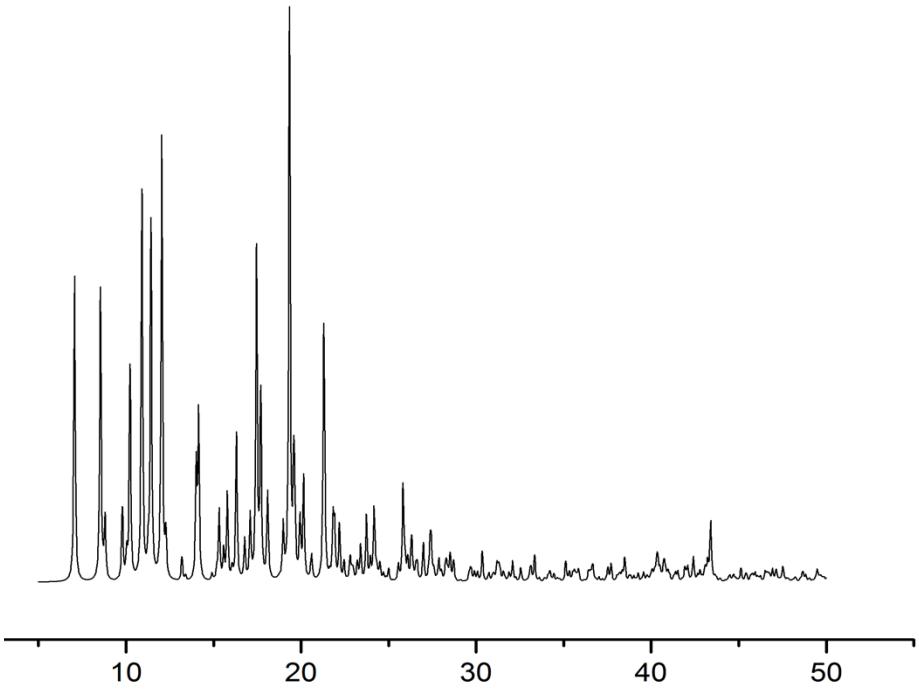

Figure S22: Simulated X-ray diffraction pattern of complex **3**

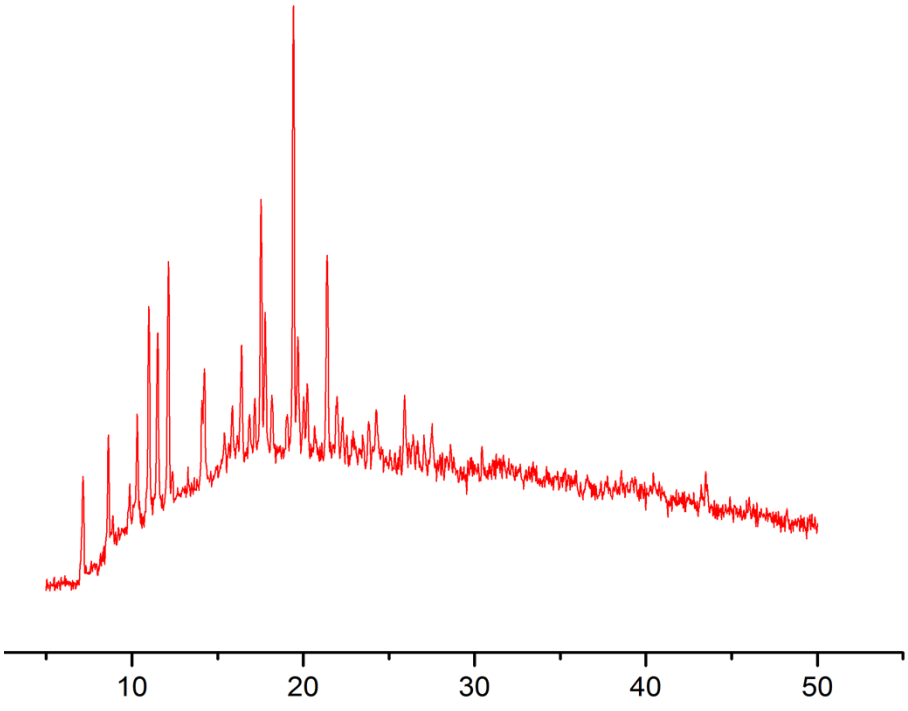

Figure S23: Powder X-ray diffraction pattern of complex **3**

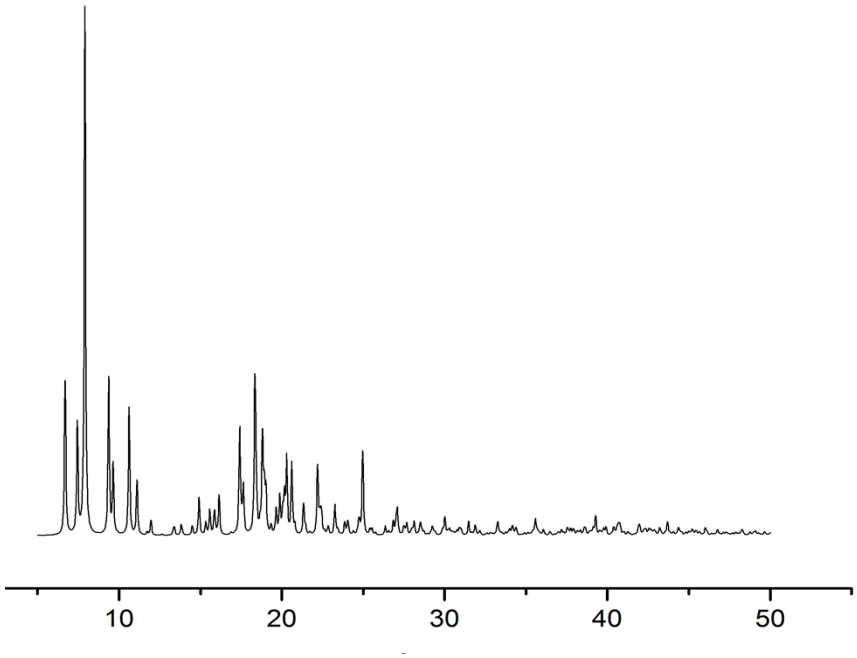

Figure S24: Simulated X-ray diffraction pattern of complex **4**

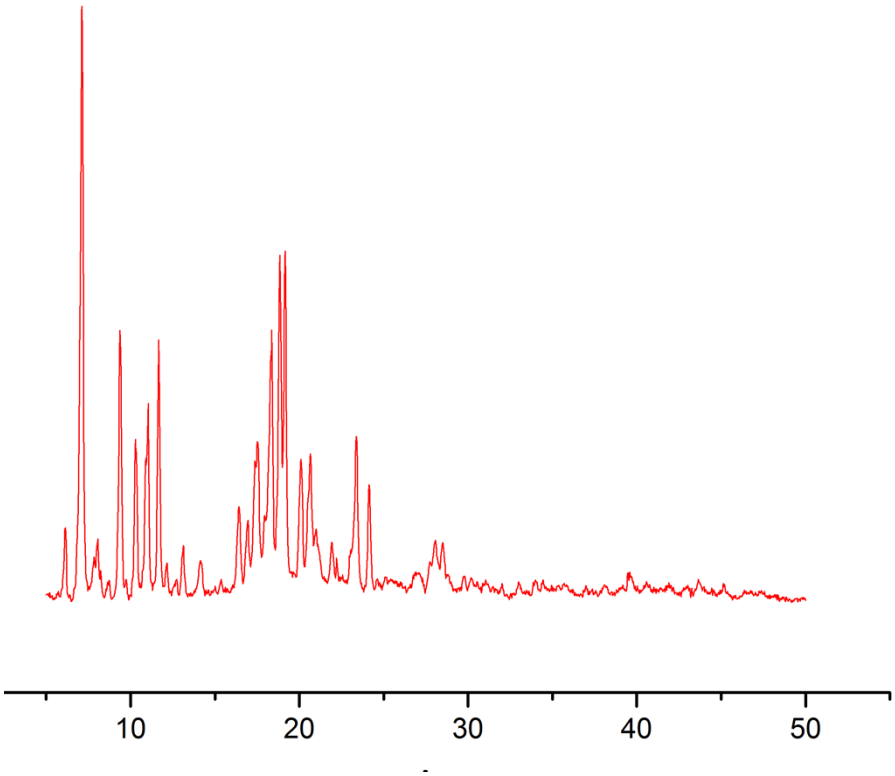

Figure S25: Powder X-ray diffraction pattern of complex **4**

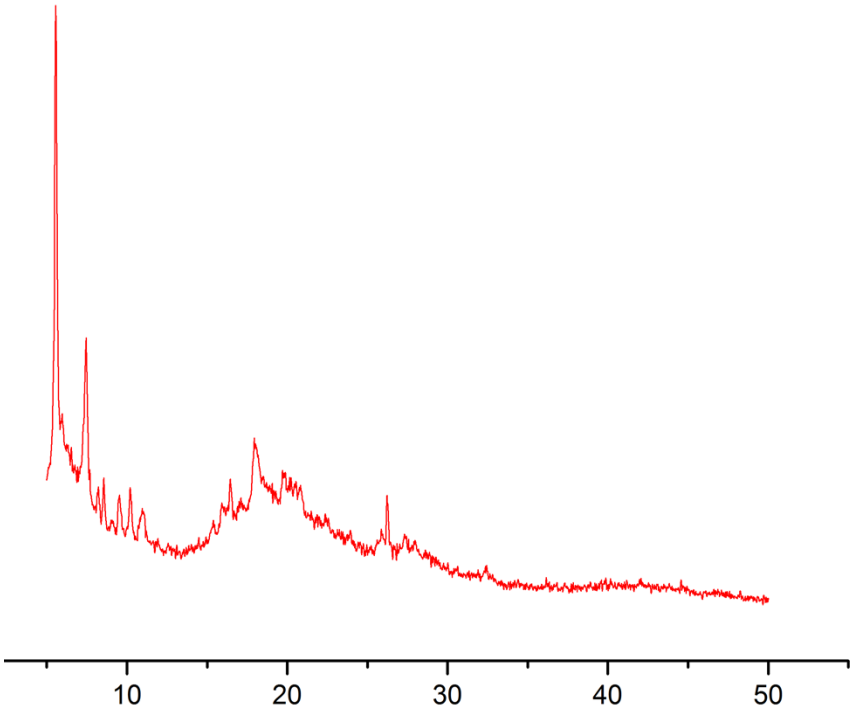

Figure S26: Powder X-ray diffraction pattern of complex **5**

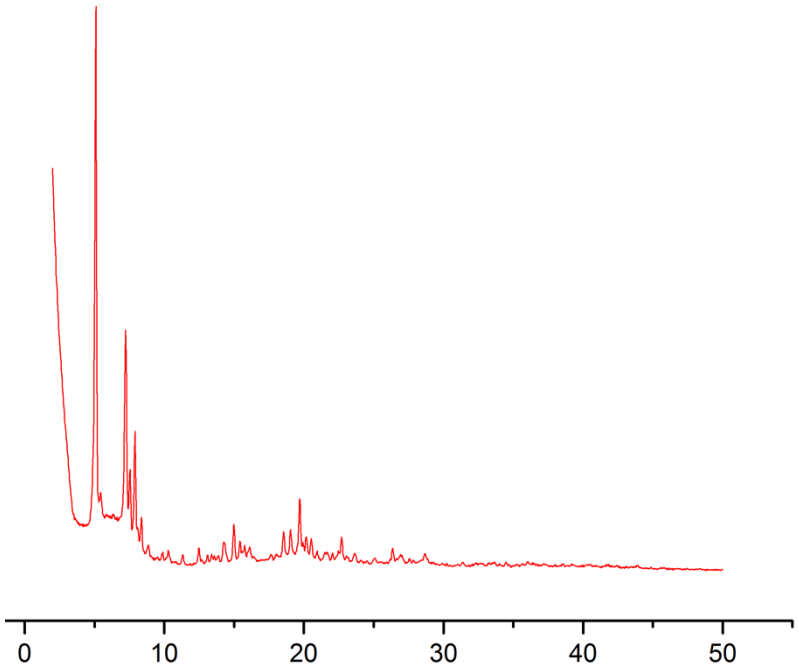

Figure S27: Powder X-ray diffraction pattern of complex **6**